American Journal of Environmental Engineering 2026, 16(1): 1-11
DOI: 10.5923/j.ajee.20261601.01

Optimization of Solution Temperature for the Plant Mediated Synthesis of ZnO Nanoparticles Using *Strychnos henningsii* Leaves Extract

Lucy J. Chebor[1,*], Lusweti Kituyi[1], Dickson Andala[2], Kiplagat Ayabei[1]

[1]Department of Chemistry & Biochemistry, University of Eldoret, Eldoret, Kenya
[2]Department of Chemistry Multimedia University, Nairobi, Kenya

Abstract The environmentally friendly and sustainable production of nanomaterials has attracted increasing attention toward green synthesis approaches as viable alternatives to conventional chemical and physical methods. In this research, zinc oxide nanoparticles (ZnO NPs) were synthesized using *Strychnos henningsii* leaf extract as a natural reducing and stabilizing agent. The phytochemical constituents present in the extract facilitated nanoparticle nucleation and growth under mild reaction conditions. The synthesis was performed at a constant pH of 8 with a reaction time of 2 h, while the temperature was varied between 40 and 70 ℃ to evaluate its influence on the structural and optical properties of the resulting nanoparticles. X-ray diffraction (XRD) was used to confirm the hexagonal wurtzite structure of ZnO, with crystallite size of 18 nm at 40 ℃ down to 14.7 nm at 70 ℃. UV-Vis spectroscopy reported a gradual decrease in optical band gap, 3.96 eV (40 ℃) to 3.37 eV (70 ℃), while photoluminescence (PL) revealed an increased and red-shifted emissions at higher temperatures. Strong Zn-O vibrations were observed, with FTIR spectra showing the participation of hydroxyl, carbonyl, and amine groups of *Strychnos henningsii* phytochemicals in reduction and capping. Overall, the results identified 70 ℃ as the optimal synthesis temperature, producing ZnO nanoparticles with superior crystallinity, reduced lattice parameters, well-defined optical absorption edges, and enhanced photoluminescence (PL) activity. Notably, this study presents the first systematic report on the optimization of temperature in green synthesis of ZnO nanoparticles using *Strychnos henningsii* leaf extract. The findings advance current understanding of plant-mediated nanomaterial fabrication and offer a sustainable pathway for engineering ZnO nanostructures for applications in photocatalysis, sensing, and optoelectronics.

Keywords Innovation, Biomedical, Global, Benign, Precursor, Biohazardous

1. Introduction

Nanotechnology has emerged as a transformative field in the 21st century, with metallic nanoparticles attracting significant attention due to their unique physicochemical properties and diverse applications across materials science, healthcare, food, and consumer industries [1,2]. In recent years, green synthesis approaches have gained prominence as environmentally friendly, cost-effective, and safe alternatives to conventional physical and chemical methods, which are often energy-intensive, toxic, and environmentally hazardous [3,6]. Among these approaches, plant-mediated synthesis offers particular advantages: plant extracts act as natural reducing and stabilizing agents, enabling rapid, high-yield production of nanoparticles under mild conditions, without the need for complex equipment or expensive reagents, thus providing a scalable and sustainable pathway for nanomaterial fabrication [4,5,7,8].

Plant extracts contain a rich diversity of phytochemicals, including polysaccharides, polyphenols, vitamins, amino acids, alkaloids, and terpenoids, which facilitate the bio-reduction of metal ions into zero-valent nanoparticles. The type and concentration of these metabolites vary across plant species and plant parts, influencing the size, morphology, stability, and functional properties of the synthesized nanoparticles [8,11]. While microbial synthesis of nanoparticles is feasible, it typically requires laborious culture maintenance, intracellular processing, and extensive purification steps, making plant-based synthesis simpler, more cost-effective, and environmentally sustainable [9,10].

Zinc oxide (ZnO) nanoparticles have attracted considerable attention due to their semiconductor properties, optical activity, and structural versatility, which underpin applications in photocatalysis, sensing, and optoelectronic devices [7,14]. Plant leaf extracts are particularly effective for ZnO nanoparticle synthesis because they provide a variety of metabolites—

* Corresponding author:
lucychebor@yahoo.com (Lucy J. Chebor)
Received: Mar. 9, 2026; Accepted: Apr. 2, 2026; Published: Apr. 8, 2026
Published online at http://journal.sapub.org/ajee

such as flavonoids, terpenoids, and saponins—that serve as both reducing and stabilizing agents. The concentration and composition of these phytochemicals critically influence nanoparticle nucleation, growth, and stability [11].

Strychnos henningsii, an African medicinal plant traditionally used to treat various diseases, snakebites, and as a tonic or flavoring agent, has recently been explored for its phytochemical richness [12,13]. However, to the best of our knowledge, no studies have systematically investigated the influence of temperature on ZnO nanoparticle synthesis using *S. henningsii* leaf extract. Temperature is a key parameter in biogenic nanoparticle synthesis, generally ranging from 40 to 80 ℃, and plays a critical role in controlling nanoparticle size, crystallinity, and optical properties [7].

This study therefore aims to synthesize ZnO nanoparticles using *S. henningsii* leaf extract as a green reducing and stabilizing agent, examining the effect of temperature on the structural and optical characteristics of the resulting nanoparticles. By elucidating the role of plant-mediated phytochemicals and reaction conditions, this work provides a sustainable approach for tailoring ZnO properties for advanced applications in photocatalysis, sensing, and optoelectronic devices.

2. Materials and Reagents

Collection of Materials

The wild plants *Strychnos heningsii* were collected from Karura Forest and further identified and confirmed by the Department of Botany, Kabarak University. Laboratory work was carried out at both Muranga and Egerton Universities.

The required chemicals, including zinc nitrate dihydrate, ethanol, and distilled water, were procured from Aldrich chemicals.

All the reagents were prepared using double-distilled water and in a glass apparatus.

Preparation of *Strychnos heningsii leaf* extract

Plant leaf material was collected, brought to the laboratory and carefully separated and cleaned using both tap water and distilled water. Samples were air-dried at room temperature for two weeks until dry then finely powdered using a blender. A 10 g of the powdered *Strychnos heningsii material* was transferred to 200 ml of distilled water in a borosil beaker and boiled with stirring using a magnetic stirrer for one hour, until the solution turned brown. The resulting mixture was then filtered using Whatman filter paper (No.1), the process repeated, to obtain a pure extract, of ZnO nanoparticles synthesis.

Green synthesis of zinc oxide nanoparticles

A 50 ml solution of 0.1 M zinc nitrate was made by dissolving zinc nitrate in deionized water in the flask filled to the mark, was then heated on a water bath at 70 ℃ for a period of 5 to 10 minutes. The heated zinc nitrate solution was blended with 30 ml of plant extract while maintaining continuous stirring. This amalgam of solutions was then maintained at a temperature of 70 ℃ for duration of 2 hours, with rigorous stirring throughout the process.

Optimization of ZnO nanoparticles

The production of metallic nanoparticles is influenced by a range of variables, including pH, temperature, capping agent concentration, incubation time, and precursor type. To attain the most optimal and effective yield of zinc oxide nanoparticles, a thorough optimization of two distinct physicochemical parameters was investigated for optimization.

Temperature Optimization

After selection of the optimum pH (8), the synthesis process was repeated using 0.1 M of zinc nitrate dihydrate and 25 ml of *strychnos henningsii* leaf extract in four different beakers. The mixture was kept under stirring at 200 rpm for different temperatures (40,50,60,70) degrees until a dark-coloured paste was observed. The paste was then cooled in an oven temperature of 100 and annealed at 500 ℃ to reduce the impurities.

Incubation Time

Contact time of reactants is also considered to be a major factor for the synthesis of a product. The synthesis of zinc oxide nanoparticles was done at four intervals of time, such as 30 minutes, 1 hour, 2 hours, and 3 hours.

Purification and Concentration of Zinc oxide Nanoparticles

The resulting precipitate was removed by employing centrifugation at 7000 rpm for 15 minutes. Eventually, the precipitate underwent a transformation from brown to a solid pale yellow colour. Subsequently, purification was carried out by sequential washing with de-ionized water, followed by oven drying, then the dried material annealed at 500 degrees for two hours to remove impurities, mashed in ceramic mortar pestle to get finer nature for characterization purposes. Ultimately, this process yielded a white-coloured powder as a final product.

Characterization of ZnO NPs

The functional groups of the ZnO NPs were characterized by Fourier transform infrared (FTIR) spectroscopy in the frequency range of 400 to 4000 cm^{-1} using a Thermo Nicolet Nexus FTIR spectrophotometer (Smart Orbit, Woodland, CA, USA). The FTIR spectra of the samples were also recorded on a 1752X spectrophotometer (Perkin Elmer, Waltham, MA, USA) using the KBr disc method.

X-ray diffraction (XRD) patterns were obtained with a PXRD-6000 diffractometer (Shimadzu, Japan) with a dwell time of 0.5 °/min. Data were recorded in the 2θ range from 4 ° to 90 ° (diffraction angle 2θ) using Cu-Kα radiation (λ = 1.5418 Å) generated at 30 kV and 30 mA. For XRD sample preparation, 10 g of sample was ground to a fine powder and deposited into a hollow space in the middle of a flat sample-holder plate. To achieve a random distribution of lattice orientations of the sample, the upper surface of the sample was well-flattened, and the XRD pattern was recorded. The same procedure was repeated for all the samples in the study.

3. Results and Discussion

Optical Analysis

The UV-Vis absorption spectra of ZnO nanoparticles synthesized at a pH of 8 for 2 hours reaction time is shown in Figure1. The spectra shows that the synthesis temperature had a strong impact on optical quality. Within the temperature range of 70 ℃, the nanoparticles displayed a sharp and well-defined absorption edge at 370 nm, which is significantly close to the bulk ZnO band gap of 3.34 eV. The specific advantage and less obvious visible-range trailing in this temperature reflected a bigger crystallinity and less surface flaw states, which is explained by the effective hydrolysis of the zinc precursors and effective capping by phytochemicals in *Strychnos henningsii*. In comparison, a spectrum at 40 ℃ indicates a diffuse edge and visible absorption tail, which implying defect-rich nanoparticles that are formed under slow reaction kinetics when incomplete reduction of the precursor and weak phytochemical interactions result in poorly ordered ZnO [17].

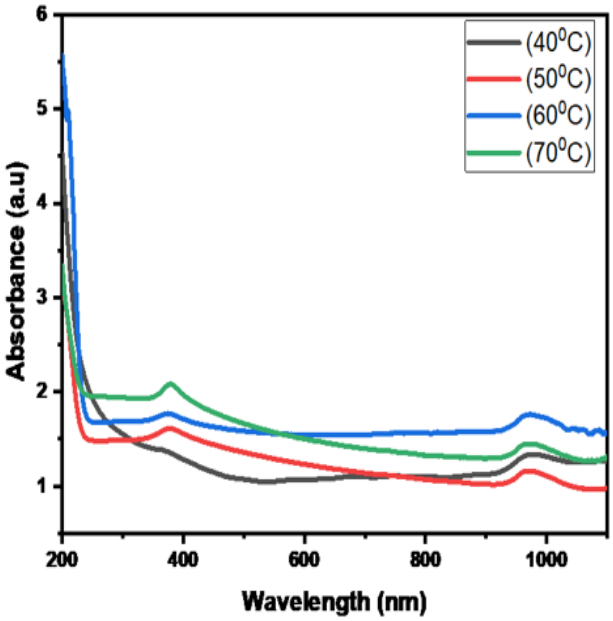

Figure 1. UV-Vis absorbance spectra of synthesized sample at different temperatures

Tauc analysis revealed a progressive decrease in band gap energy as temperature increased: 3.96 eV (40 ℃), 3.74 eV (50 ℃), 3.50 eV (60 ℃), and 3.37 eV (70 ℃). This decrease in band gap with temperature could be attributed to an increase in both crystallinity and particle density, and a decrease in defect-related localized states, which permit electronic transitions nearer to the intrinsic band edge [18]. On the other hand, an excessively high band gap, at 40 ℃, indicates quantum confinement effects because of high defect density and low crystallinity, which curves the absorption edge [19]. Band gap tuning is defined as a comparable narrowing of band gaps as the synthesis temperature is increased, For instance, green-synthesized ZnO using *Cymbopogon citratus* exhibited a decrease in band gap from 0.5 to 0.4 eV as the synthesis temperature was raised [20]. Other comparable reductions were also observed in ZnO synthesized using *Ocimum lamifolium* extracts in which band gaps reduced with temperature increase as the extract improved more compact nucleation and reduced surface disorganization [21].

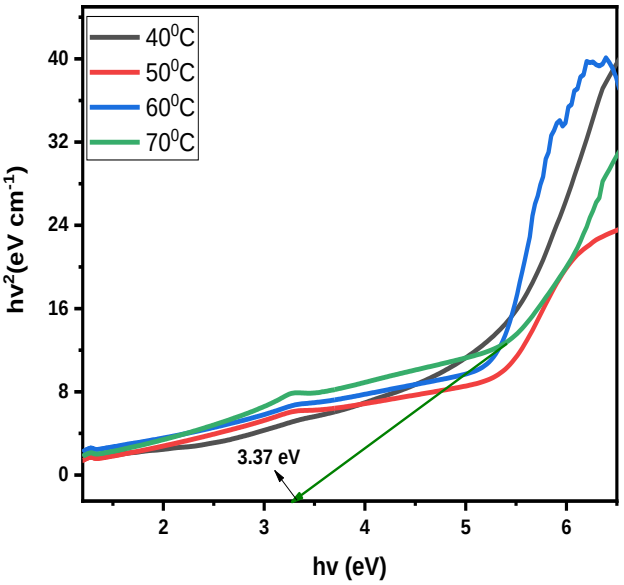

Figure 2. Shows UV-Vis Tauc plot extrapolated band gaps of synthesized samples

These values are also in agreement with other reported values of green-synthesised ZnO systems. [22] found out a band gap near 3.42 eV of ZnO prepared by using Licania tomentosa extract, comparable to 3.37 eV at 70 ℃ in these experimental results. According to ŞiMşek et al. (2022), ZnO mediated by plants usually has band gaps in the range of 3.2 to 3.6 eV based on crystallite size and defect content, which entirely overlap with the range here. Likewise, Zagorac et al. (2022) reported temperature-dependent narrowing of band gaps in Alnus nepalensis in mediation by ZnO, which corroborates the interpretation of greater synthesis temperature preferring high-quality, near-bulk band gaps. Together, these comparisons prove that the findings measured using Srychnos henningsii are not only consistent with, but also competitive to the more well-studied plants in the green synthesis of ZnO.

Table 1 presents extrapolated band gaps of synthesized materials of temperatures 40-60.

Table 1. Extrapolated band gaps of synthesized samples at varying temperatures

Temperature (℃)	Band Gap (eV)
40	3.96
50	3.74
60	3.50
70	3.37

The results indicate that 70 ℃ is the optimal synthesis temperature under constant pH and reaction time, producing ZnO nanoparticles with the narrowest, bulk-like band gap,

the steepest absorption edge, and minimal visible defect-related absorption. In contrast, synthesis at 40 ℃ yielded nanoparticles with inferior optical quality, characterized by extended absorption tails and an overestimated band gap, reflecting structural disorder and incomplete hydrolysis. [23]. The novelty of the research is in the fact that it is the first synthesis route that demonstrate that *Strychnos henningsii* phytochemicals could be used to control temperature-driven optical changes in ZnO nanoparticles. This observation offers a plant-specific model of customizing band gap and optical quality by reaction conditions, and thus as part of the facilitation of the green-synthesized ZnO towards photocatalytic, optoelectronic, and sensing purposes as observed in related research by other research groups [24,25].

Photoluminescence

Photoluminescence spectra of the ZnO nanoparticles prepared using *Strychnos henningsii* extract, is shown in Figure 3. The spectra exhibit high emission bands at the blue-green region (448-496 nm), typical of defect-related transitions in wurtzite ZnO. These emissions could be largely attributed to inherent point defects like oxygen vacancies (V_O), zinc interstitials (Zni), and their complexes, serving as radiative recombination centres [19]. The difference in the peak position and intensity with change in temperature proves that thermal energy during synthesis regulates defect formation, surface passivation and crystallinity [25]. It is augmented by the use of *Strychnos henningsii* phytochemicals, which are enriched with alkaloids, terpenoids, and phenolics, as these natural molecules not only reduced by Zn^{2+} to form ZnO, but also cap growing crystallites, which tunes luminescent defect states density [26].

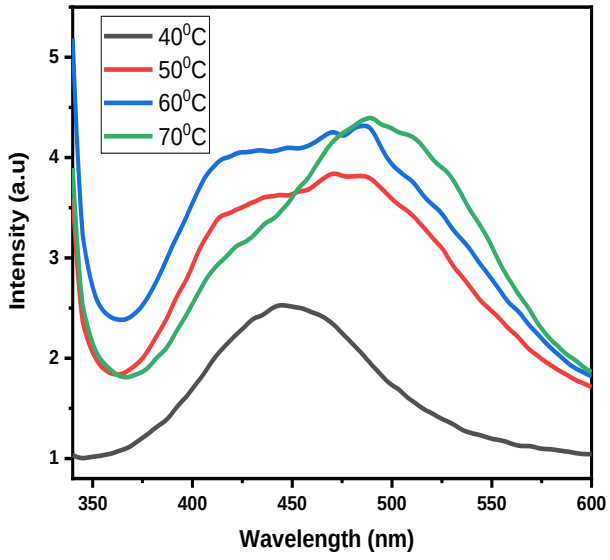

Figure 3. Photoluminescence (PL) spectra of synthesized sample at different temperatures

The peak emission that appeared at 448 nm with low intensity (2.2 a.u.) at 40 ℃, suggests that the nanoparticles were poorly crystallized and had low radiative recombination. This could be credited to slow hydrolysis as well as incomplete reduction, leading to larger particles involving defects, but with non-radiative processes prevailing over the recombination process. Conversely, an increase in temperature during synthesis can cause an increase in the emission peaks to longer wavelengths: 463 nm at 50 ℃, 492 nm at 60 ℃ and 496 nm at 70 ℃, and intensities increased to 3.8-4.3 a.u. The temperature-dependent red shift of the emission indicates the increase in the defect complexity and the decrease in the depth of the donor-acceptor pair recombination, whereas the higher intensity indicates the higher crystallinity and the larger number of centers with optically active sites [27]. The peak emission at 70 ℃ is comparable to those of the XRD and UV- Vis data, which means that the temperature provides the highest crystalline quality and the most successful contact of phytochemicals with ZnO surfaces.

Table 2 below shows emission wavelengths and intensities of synthesized materials.

Table 2. Emission wavelengths and intensities of synthesized samples

Temperature (℃)	Emission Wavelength (nn)	Intensity (a.u)
40	448	2.2
50	463	3.8
60	492	4.1
70	496	4.3

The deconvoluted spectrum at 70 ℃, shown in Figure 4, displays several components including a feature at approximately 414 nm and 442 nm is related to a transition of Zni and weak donor states; the high band at about 484 nm is due to singly ionized oxygen vacancies (V_O), with the larger emission at 540 nm and above being due to deep-level oxygen-related defects [28].

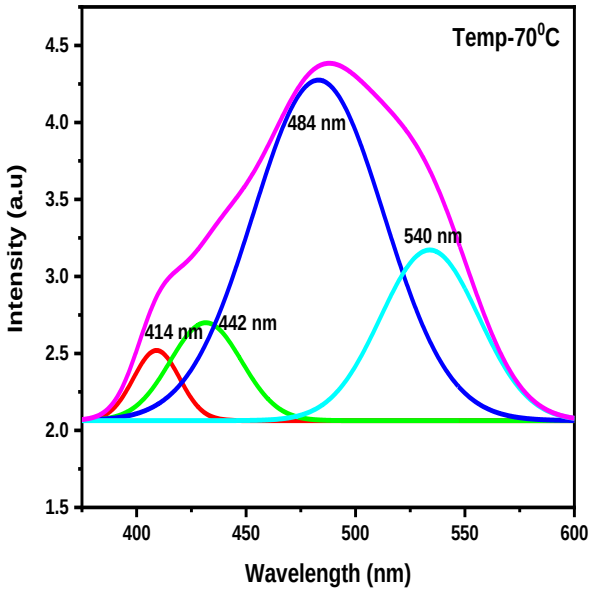

Figure 4. Gaussian deconvolution of synthesized sample at 70 ℃

The prevalence of the 484 nm peak indicates that oxygen vacancies are the main luminescent centres in these

green-synthesized ZnO nanoparticles. Notably, the increased concentration and reduced dispersion of these emissions at 70 ℃ indicate that an optimized temperature facilitates a targeted defect formation instead of a random occurrence of non-radiative defects. It means that the phytochemical-rich conditions of *Strychnos henningsii* not only permit reduction and stabilization but also selectively passivate non-radiative states and retain useful optical defects.

The trends of the PL observed have been in line with other reports of temperature-dependent PL in plant-mediated ZnO systems. ZnO nanoparticles produced using the extract of *Cymbopogon citratus* exhibited blue-green emissions of approximately 450-500 nm, with the intensity of the emission becoming higher as the synthesis conditions enhanced the crystallinity quality [29]. Likewise, ZnO synthesized using *Alnus nepalensis* exhibited improved PL intensity and red-shifted emission when the synthesis conditions were biased towards smaller, more ordered crystallites [27]. Jayachandran *et al*. (2021) identified a peak of ZnO emission rate of 470-500 nm with Licania tomentosa, which matches the range of this experiment at 60-70 ℃. These similarities verify that the best optical quality at 70 ℃ with *Strychnos henningsii* is consistent and even better in other cases than more familiar plant systems, with which better ZnO systems in green synthesis have been more commonly used.

This study presents a demonstration of the first instance of temperature tuning at constant pH of 8 on PL emission of ZnO synthesized using the *Strychnos henningsii* extract. The evidence indicates clearly that 40 ℃ yields the worst quality nanoparticles, weak PL intensity and shorter wavelength emission, whereas 70 ℃ yields the most structured emission, which is a strong one with high crystallinity and error control of its defects. The originality is the first direct connection of the phytochemical-mediated conditions of synthesis and defect-related optical emission, which places *Strychnos henningsii* in the position of a sustainable and efficient plant source of ZnO with specific PL characteristics. These results underscore that enhanced green synthesis at 70 ℃ is capable of producing ZnO nanoparticles that can be used in photocatalysis, optoelectronics, and sensing, where defect states control and high crystallinity are vital [30].

FTIR Analysis

The FTIR spectra of ZnO nanoparticles prepared with a *Strychnos henningsii* extract at various temperatures (40 to 70 ℃) confirms that the phytochemicals take part in the reduction and stabilization of the nanoparticles. In all spectra, a broad absorption band in the range of 3200-3500 cm-1 could be attributed to O-H stretching vibrations of hydroxyl groups of phenols and alcohols found in the extract and adsorbed water [31]. These hydroxyl groups are hydrogen donors and stabilizers when making nanoparticles. Bands under 1600-1700 cm^{-1} are related to C=O stretching vibrations of carbonyl groups, which are part of flavonoids and alkaloids, and contribute to the reducing capacity of Zn^{2+} ions and to the binding to the surface of the nanoparticle [32]. Feeble bands at 1400-1450 cm^{-1} region are associated with C-N stretching of the amino acids and potential symmetric stretching of the -COO- groups, indicating the presence of amino acids and proteins in the stabilization procedure of the ZnO nanoparticles [33].

Figure 5 presents FTIR spectra of synthesized samples at different temperatures.

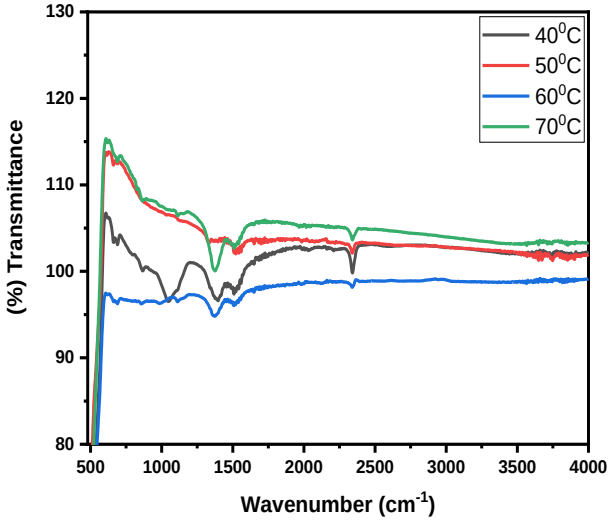

Figure 5. FTIR spectra of synthesized samples at different temperatures

The most significant signature is the extreme absorption band under the 600 cm^{-1} threshold, as it represents the stretching vibration of Zn-O bonds, and it proves the effective synthesis of the ZnO nanoparticles [19]. The sharpness of this band increased with temperature, particularly at 70 ℃, implying better crystallinity and maximum conversion of precursor salts to ZnO. The weaker signal of Zn-O at 40 ℃ is, by comparison, an indication of incomplete reduction and degradation in the formation of Zn-O networks, which agrees with the XRD and UV-Vis data indicating broader peaks and an increase in band gap at this temperature.

The retention of the phytochemical capping groups was also affected by temperature, despite not affecting Zn-O bond strength. Stronger O-H and C=O bands at 40 ℃ show increased retention of organic functional groups on the nanoparticle surface, which is explained by a lack of complete reaction and a weak interaction of phytochemicals with the crystalline structure. These bands became weaker at higher temperatures (60-70 ℃), suggesting greater breakdown of labile groups and greater formation of Zn-O networks, although they had enough phytochemical residues left to confer agglomeration stability. This is in line with prior reports of ZnO synthesized using *Ocimum lamifolium* and *Cymbopogon citratus*, whereby higher synthesis temperature minimised residual organic peaks and sharpened the Zn-O signature [21].

The phytochemical-ZnO interactions in this case are consistent with the other plant-mediated systems. ZnO nanoparticle synthesized with *Licania tomentosa* exhibited comparable O-H, C=O and Zn-O signatures, and this is important to demonstrate the universal role of phenols, alkaloids and carboxylates to mediate nanoparticle synthesis.

The FTIR bands also validated the role of carbonyls, hydroxyls, and amines in the synthesis process in Alnus nepalensis mediated ZnO, which is very similar to the current results with *Strychnos henningsii* [34]. Such comparisons confirm that the functional groups identified here are the same as those of recent green ZnO literature, and the systematic analysis of temperature effects with *Strychnos henningsii* offers new information not previously present in the literature.

From these FTIR results, the formation of ZnO nanoparticles was most favourable at 70 ℃. Zn-O bond vibrations were higher, and organic residue bands were smaller, which means that phytochemicals mediate the reduction and stabilization process most effectively. In contrast, 40 ℃ results provided nanoparticles with weak Zn-O signatures and strong organic bands, which testify to poor conversion and poor crystallization. The novelty of the work is the determination of the interaction of the phytochemicals of the rarely studied species *Strychnos henningsii* with Zn^{2+} ions at different synthesis temperatures to guide the formation of nanoparticles. This vegetal intuition indicates that *Strychnos henningsii* can serve both as a green reductant and as a stabilizer and allow temperature control to obtain the best nanoparticle characteristics [48].

XRD Analysis

Figure 6 shows XRD pattern of ZnO nanoparticles at various temperatures (40-70 ℃) synthesized with *Strychnos henningsii* leaf extract. All diffraction peaks could be indexed to the hexagonal wurtzite phase of ZnO (JCPDS 01-070-8072). The lack of anKary secondary phases proved that the phytochemicals in the extract were used efficiently as reducing and stabilizing agents, which allowed one to obtain pure ZnO even when the reaction conditions were changing. This result aligns with recent reports in which flavonoids, alkaloids, and phenolics contained in plant extracts were found to be instrumental in the stabilization of wurtzite ZnO nuclei during the process of green synthesis [34].

The effect of temperature was very clearly observed in the 2θ shifts, the lattice parameters, and crystallite sizes. At 40 ℃, the (101) reflection was observed at 38.39 °with a d-spacing of 2.3447 Å, with a = 3.0776 Å and c = 4.9313 Å, where symbol Å, is the Angstrom unit. These were higher lattice values, attributed to slow hydrolysis of zinc precursors and low temperature condensation with ineffective condensation leading to incomplete crystallization and inclusion of defects. At 70 ℃, on the other hand, the maximum shifted to a value of 38.45 °, which gives the shortest d-spacing (2.3412 A), and the shortest lattice constants (a = 3.0729 A and c = 4.9239 A). This decrease in lattice is explained by the increased ability to hydrolyze and condense Zn-OH intermediates and the increase in coordination of phytochemicals, which allows the Zn-O tetrahedra to be brought closer to each other [21]. Therefore, the compactness of the ZnO lattice and long- ange order were enhanced by increasing temperature, and 70 ℃ presented the optimal temperature.

The crystallite size D (nm) from Scherrer equation analysis also exhibited a high temperature dependence. The mean size was 17.98 nm at 40 ℃, which gradually reduced to 14.71 nm at 70 ℃. This decrease is explained by accelerated nucleation at higher temperatures, with more nuclei being produced but their development being inhibited by phytochemical capping to form smaller coherently diffracting domains. The observed simultaneous temperature dependence of microstrain (0.0059 - 0.0072) and dislocation density (0.00309 – 0.00462 nm^{-2}) indicates the integration of minor lattice distortions, which is a normal consequence of nanocrystals, and does not reduce the quality of the phases [35]. Rather, a smaller particle size and acceptable strain at 70 ℃ are more favourable to balance catalytic and optical applications where defect-mediated reactivity is a desirable property. A summary of 2 θ, FWHM and crystallite sizes of synthesized samples is in Table 3.

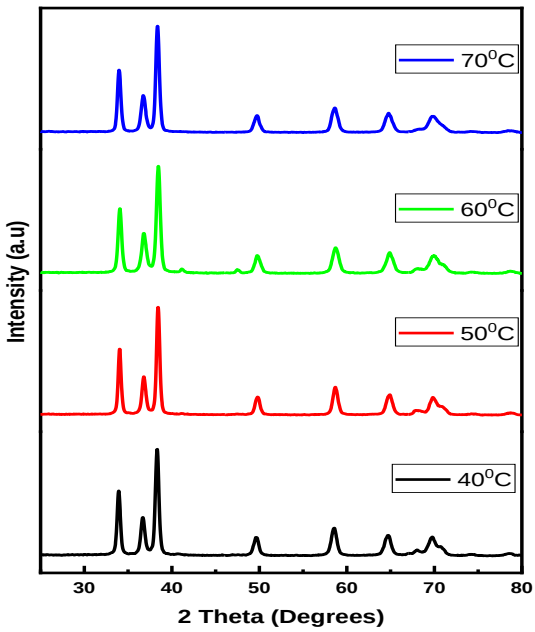

Figure 6. XRD pattern of synthesized samples at different temperatures

Table 3. Summarized 2 θ, FWHM, crystallite sizes of synthesized samples

Temperature (℃)	2θ (Degrees)	FWHM (°)	Crystallite size D (nm)	Dislocation (nm^{-2})	Strain
40	38.39	0.4682	17.98	0.00309	0.00587
50	38.36	0.5190	16.22	0.00380	0.00651
60	38.31	0.5198	16.19	0.00380	0.00653
70	38.45	0.5723	14.71	0.00462	0.00716

The obtained crystallite size values (14.7-18.0 nm) are consistent with other green synthesis studies when compared with the recent literature. As an example, ZnO prepared with the extract of *Licanas tomentosa* produced crystallites with a length of approximately 12.4 nm, which is a little smaller but nevertheless in the same range [36]. ZnO synthesized with Cymbopogon citratus leaf extract had crystallite sizes of approximately 19 nm, which are similar to those of reported in this study in lower-temperature samples [37]. Similarly, reports on ZnO nanoparticles synthesized using *Justicia adhatoda* indicate crystallite sizes ranging from 12 to 20 nm, which is consistent with the findings of the present study [38]. The results described in this research are consistent with the existing body of literature, but parallel studies are still rather few. This work has shown that Strychnos henningsii extract can be used to synthesize ZnO nanocrystals with structure similar to those prepared using other, more frequently studied plant sources. This fact points to the novelty and efficiency of the current green synthesis method.

FWHM is a measure of how broad or sharp diffraction peaks are, larger values indicate broader peaks, which implies smaller crystalline size in the crystal lattice [39]. This peak broadening is associated with finite crystal and the lattice distortion that disrupts the crystal's ideal periodicity. As recorded in Table 3, an inverse relationship between FWHM and crystallite size was observed as synthesis temperature was increased. FWHM gradually increased, whereas the crystallite size consistently decreased. This particular observation is not unusual since, Sherrer's equation illustrates an inverse relationship between these two variables, crystallite size, D and FWHM. Similar trend has been reported in recent XRD studies of metal oxide nanoparticles [40,41]. These studies reported that at lower processing temperature, larger crystallites yielded narrower peaks, and as the working temperatures were adjusted upwards, peaks broadened. They attributed the later observation to increased lattice distortion on defect formation. Further, Table 3 reveal the increase in dislocation density with decrease in crystallite size. This observation is expected since dislocation is a measure of length distortion per unit volume, given by Equation 1, a relation that was initially used by Kotresh et al, (2021) [50].

$$\text{Dislocation density } (\delta) = \frac{1}{D^2}$$

Thus, according to this relation, smaller grains tend to have more defects per unit volume, or rather more dislocations [50]. This observation also aligns with findings of various research groups [42,43], who reported increased dislocation and for smaller crystallite size in crystals of metal oxide nanoparticles with increasing calcination temperatures.

Lattice strain contributes to XRD peak broadening in the same way small crystallite does [44] Strain emanates from the distortion of the crystal lattice in the form of defects, mismatch between planes and sometimes from dislocations [45]. Data in Table 3 reports a direct variation between microstrain and synthesis temperature. Notable, strain increased with increase in processing temperature. An indication of increased lattice distortion i.e. existence of imperfections such as defects of stacking faults at higher temperatures. These findings are consistent with those reported by Al-Hazmi et al, (2022) [38], a study that also revealed a close link between strain (or small size) and XRD peak broadening.

Table 4 shows calculated d-spacing, and lattice parameters of synthesized samples at temperature values.

Table 4. Calculated d-spacing, and lattice parameters of synthesized samples at different temperatures

Temperature (℃)	2θ (Degrees)	d-spacing (Å)	a (Å)	c (Å)
40	38.39	2.3447	3.0776	4.9313
50	38.36	2.3465	3.0799	4.935
60	38.31	2.3494	3.0837	4.9412
70	38.45	2.3412	3.0729	4.9239

Generally, the results of XRD indicate that 40 ℃ provides the lowest crystalline quality, expanded lattice parameters, larger crystallites, and reduced defect incorporation owing to low reaction kinetics. On the other hand, an optimum temperature of synthesis of 70 ℃ would yield high crystallinity, reduced nanocrystal size (14.7 nm), decreased lattice parameters, and tolerable strain and dislocation density. This optimization of structure based on temperature regulation at a constant pH (8) and synthesis time (2h) underscores the significance of both the reaction environment and exclusive phytochemicals of *Strychnos henningsii* in shaping ZnO nanoparticles to meet the high surface activity and unstable crystallinity requirements.

The diffraction peak at around 38 ° slightly change as the temperature rises, as it goes down to 38.39 ° at 40 then to 38.31 ° at 60℃ and then back to 38.45° at 70℃. Bragg law states that a decrease in 2 theta is proportional to an increase in interplanar spacing and this is supported by the fact that, d-spacing increases by 2.3447 Å (40℃) to 2.3494 Å (60℃). The peak at 70℃ is however shifted to higher angle with a decrease in d-spacing to 2.3412 Å.

The presence of such peak shifts is usually explained by the lattice strain and redistribution of defects in nanostructured oxides often caused by temperature. Recent research on ZnO and other metal oxide nanoparticles reported that diffraction angle shifts towards lower angles usually suggest lattice expansion as a result of tensile strain or relaxation effects on the surface, and shifts towards higher angles suggest lattice contraction because of compressive strain or annealing of defects [46,47]. The current tendency indicates that intermediate temperature gain (to 60℃) facilitates an inconsiderable lattice expansion which can be attributed to defects introduction or surface strain results in nanoscale crystallites.

Lattice parameters also confirm this interpretation. The parameters, a and c are both rising gradually with increasing temperature (40℃, a = 3.0776 Å, c = 4.9313 Å and 60℃, a = 3.0837 Å, c = 4.9412 Å). Related studies have also shown similar temperature induced changes in lattice constants, where nanoparticles systems have shown increased lattice dimensions caused by strain and defects at intermediate synthesis

temperature [48,49]. The surface atoms in nanoparticles have less coordination and this may cause outward relaxation and slightly increased lattice parameters than the bulk structures.

SEM analysis

The surface morphology of the synthesized ZnO nanoparticles was examined using scanning electron microscopy (SEM). Images were recorded at a magnification of 3000×, as shown in Figure 7. The image showed spherical shape nanoparticles formed with diameter range 12-25 nm. SEM revealed the particle to have highly aggregated and porous morphology with closely packed nanograins. The texture appears rough and the substructures appears to have irregular spherical shapes typical for non-uniform growth mechanism. The irregular particles could be as a result of agglomeration of tiny primary crystallites. The partially agglomerated state could partly be due to the fact that no hard-acting chemical filtration methods were employed in green synthesis, and partly due to the smaller size of the nanoparticles [51]. But, the nanoparticles are not well resolved at the specified magnification, this means that the crystallite size is smaller than the micrometer scale of the observed aggregates. This observation agrees with the crystallite sizes obtained from XRD analysis. The observed aggregation behavior is common in green synthesized ZnO nanoparticles using algae [52] and fruit extracts [53]. These studies attributed the observed aggregation to hydrogen bonding, van der Waals interaction and high surface energy of the particles associated with plant mediated synthesis of nanoparticles.

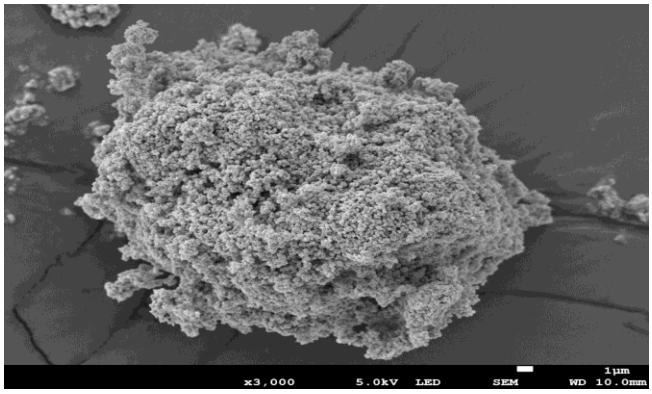

Figure 7. SEM micrograph of biosynthesized ZnO

TEM analysis

Transmission electron microscopy (TEM) images clearly demonstrate that the ZnO nanoparticles produced through biosynthesis exhibit a distinctive rod-like morphology, characterized by a tightly constrained size distribution, as depicted in Figure 8. The diameter of these ZnO nanoparticles spans a range from 9.6 nm to 25.5 nm. Remarkably, the dimensions of the ZnO nanoparticles in this study closely mirror those obtained through biosynthesis using leaf extracts of *Parthenium hysterophorus* L, *Aloe barbadensis*, and *Poncirus trifoliate*. This consistency underscores the reproducibility of the biosynthesis method across diverse botanical sources and emphasizes the potential utility of this approach in generating nanoparticles with controlled and desirable properties. The agglomerate surface is rough and porous, with the nature of the surface indicating that the nucleation process took place quickly and the particles grew and coalesced during the synthesis. The lack of rod-shaped or hexagonal platelet morphology reveals that there is no crystal growth which is isotropic with the chosen calcination temperature. This presents a striking consistency with observed finding by various research groups [54-57].

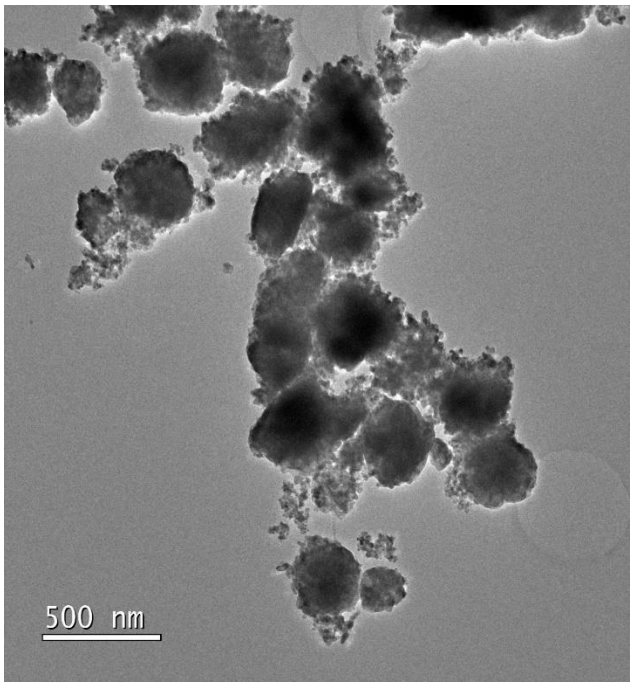

Figure 8. TEM image of biosynthesized nano ZnO

4. Conclusions

The results of this paper show the possibility of green synthesis of nanoparticles using *Strychnos henningsii* leaf extract as a natural reducing and stabilizing reagent and systematically assessing the impact of synthesis temperature (40-70 ℃) with a constant pH 8 and reaction time of 2 h. The results have conclusively demonstrated that the optimum synthesis temperature is 70 ℃ and the nanoparticles synthesized under this temperature had better structural and optical properties than those synthesized at lower temperatures.

XRD analysis confirmed that all samples crystallized in the hexagonal wurtzite structure of ZnO, consistent with JCPDS 01-070-8072, with no secondary phases detected. Nanoparticles synthesized at 70 ℃ exhibited the lowest lattice parameters (a = 3.0729 Å, c = 4.9239 Å), the smallest crystallite size (14.7 nm), the highest strain and dislocation density, and clear evidence of densely nucleated particles with enhanced crystallinity. In contrast, synthesis at 40 ℃ produced larger, defect-rich crystallites (18 nm) with increased lattice parameters, indicating lower structural quality. These results highlight the critical role of reaction temperature in determining the structural quality of ZnO nanoparticles

under green synthesis conditions: 70 ℃ yields highly crystalline, optically active, and defect-controlled nanoparticles, whereas 40 ℃ produces nanoparticles of inferior structural and optical quality.

ACKNOWLEDGEMENTS

The authors wish to thank Murang'a University for offering various analytical techniques.

Conflict of Interest

No conflict of interest.

REFERENCES

[1] A. G. Kaningini et al., "Effect of Optimized Precursor Concentration, Temperature, and Doping on Optical Properties of ZnO Nanoparticles Synthesized via a Green Route Using Bush Tea (Athrixia phylicoides DC.) Leaf Extracts," ACS Omega, vol. 7, no. 36, pp. 31658–31666, Sep. 2022, doi: 10.1021/acsomega.2c00530.

[2] H. M. Saleh and A. I. Hassan, "Synthesis and Characterization of Nanomaterials for Application in Cost-Effective Electrochemical Devices," Sustainability, vol. 15, no. 14, p. 10891, Jul. 2023, doi: 10.3390/su151410891.

[3] S. Ying et al., "Green synthesis of nanoparticles: Current developments and limitations," Environ. Technol. Innov., vol. 26, p. 102336, May 2022, doi: 10.1016/j.eti.2022.102336.

[4] J. Jalab, W. Abdelwahed, A. Kitaz, and R. Al-Kayali, "Green synthesis of silver nanoparticles using aqueous extract of Acacia cyanophylla and its antibacterial activity," Heliyon, vol. 7, no. 9, p. e08033, Sep. 2021, doi: 10.1016/j.heliyon.2021.e08033.

[5] N. C. Nkosi, A. K. Basson, Z. G. Ntombela, N. G. Dlamini, and R. V. S. R. Pullabhotla, "Green synthesis and characterization of iron nanoparticles synthesized from bioflocculant for wastewater treatment: A review," Biotechnol. Notes, vol. 6, pp. 10–31, 2025, doi: 10.1016/j.biotno.2024.12.001.

[6] P. Kumari, A. Srivastava, R. K. Sharma, D. Sharma, and S. K. Srivastava, "Zinc Oxide: A Fascinating Material for Photovoltaic Applications," in Nanomaterials for Innovative Energy Systems and Devices, Z. H. Khan, Ed., Materials Horizons: From Nature to Nanomaterials, Singapore: Springer Nature Singapore, 2022, pp. 173–241. doi: 10.1007/978-981-19-0553-7_6.

[7] R. Saxena et al., "A review on green synthesis of nanoparticles toward sustainable environment," Sustain. Chem. Clim. Action, vol. 6, p. 100071, Jun. 2025, doi: 10.1016/j.scca.2025.100071.

[8] J. Pan, H. Qian, Y. Sun, Y. Miao, J. Zhang, and Y. Li, "Microbially synthesized nanomaterials: Advances and applications in biomedicine," Precis. Med. Eng., vol. 2, no. 1, p. 100019, Mar. 2025, doi: 10.1016/j.preme.2025.100019.

[9] M. M. Abady, D. M. Mohammed, T. N. Soliman, R. A. Shalaby, and F. A. Sakr, "Sustainable synthesis of nanomaterials using different renewable sources," Bull. Natl. Res. Cent., vol. 49, no. 1, p. 24, Apr. 2025, doi: 10.1186/s42269-025-01316-4.

[10] D. C. Bouttier-Figueroa, J. M. Cortez-Valadez, M. Flores-Acosta, and R. E. Robles-Zepeda, "Synthesis of Metallic Nanoparticles Using Plant's Natural Extracts: Synthesis Mechanisms and Applications," Biotecnia, vol. 25, no. 3, pp. 125–139, Oct. 2023, doi: 10.18633/biotecnia.v25i3.1916.

[11] M. Y. Al-darwesh, S. S. Ibrahim, and M. A. Mohammed, "A review on plant extract mediated green synthesis of zinc oxide nanoparticles and their biomedical applications," Results Chem., vol. 7, p. 101368, Jan. 2024, doi: 10.1016/j.rechem.2024.101368.

[12] E. K. Tirop, N. N. Maina, J. K. Maina, P. K. Njenga, E. Magiri, and V. W. Ngumi, "Evaluation of Toxicity of Strychnos henningsii (Gilg) (Loganiaceae) Leaves and Root Aqueous Extracts in Mice," Eur. J. Med. Plants, vol. 25, no. 1, pp. 1–11, Sep. 2018, doi: 10.9734/EJMP/2018/43613.

[13] C. Zhu and X. Wang, "Nanomaterial ZnO Synthesis and Its Photocatalytic Applications: A Review," Nanomaterials, vol. 15, no. 9, p. 682, Apr. 2025, doi: 10.3390/nano15090682.

[14] G. Philippe, L. Angenot, M. Tits, and M. Frédérich, "About the toxicity of some Strychnos species and their alkaloids," Toxicon, vol. 44, no. 4, pp. 405–416, Sep. 2004, doi: 10.1016/j.toxicon.2004.05.006.

[15] P. B. Mallikharjuna, L. N. Rajanna, Y. N. Seetharam, and G. K. Sharanabasappa, "Phytochemical Studies of Strychnos potatorum L.f. – A Medicinal Plant," J. Chem., vol. 4, no. 4, pp. 510–518, Jan. 2007, doi: 10.1155/2007/687859.

[16] A. N. Abdulqodus et al., "Green synthesis of ZnO nanoparticles: effect of pH on morphology and photocatalytic degradation efficiency," Appl. Phys. A, vol. 131, no. 9, p. 720, Sep. 2025, doi: 10.1007/s00339-025-08874-4.

[17] S. Kumar, V. Singh, and A. Tanwar, "Structural, morphological, optical and photocatalytic properties of Ag-doped ZnO nanoparticles," J. Mater. Sci. Mater. Electron., vol. 27, no. 2, pp. 2166–2173, Feb. 2016, doi: 10.1007/s10854-015-4227-1.

[18] S. Raha and Md. Ahmaruzzaman, "ZnO nanostructured materials and their potential applications: progress, challenges and perspectives," Nanoscale Adv., vol. 4, no. 8, pp. 1868–1925, 2022, doi: 10.1039/D1NA00880C.

[19] A. S. Abdelbaky et al., "Green approach for the synthesis of ZnO nanoparticles using Cymbopogon citratus aqueous leaf extract: characterization and evaluation of their biological activities," Chem. Biol. Technol. Agric., vol. 10, no. 1, p. 63, Jul. 2023, doi: 10.1186/s40538-023-00432-5.

[20] E. Tilahun, Y. Adimasu, and Y. Dessie, "Biosynthesis and Optimization of ZnO Nanoparticles Using Ocimum lamifolium Leaf Extract for Electrochemical Sensor and Antibacterial Activity," ACS Omega, vol. 8, no. 30, pp. 27344–27354, Aug. 2023, doi: 10.1021/acsomega.3c02709.

[21] M. Thiam et al., "Green Synthesis of ZnO Nanoparticles Using Licania tomentosa Benth (Oiti) Leaf Extract: Characterization and Applications for the Photocatalytic Degradation of Crystal Violet Dye," Processes, vol. 13, no. 3, p. 880, Mar. 2025, doi: 10.3390/pr13030880.

[22] T. Şimşek, A. Ceylan, G. Ş. Aşkin, and Ş. Özcan, "Band Gap Engineering of ZnO Nanocrystallites Prepared via Ball-

Milling," Politek. Derg., vol. 25, no. 1, pp. 89–94, Mar. 2022, doi: 10.2339/politeknik.647702.

[23] D. Zagorac et al., "Band Gap Engineering of Newly Discovered ZnO/ZnS Polytypic Nanomaterials," Nanomaterials, vol. 12, no. 9, p. 1595, May 2022, doi: 10.3390/nano12091595.

[24] F. B. Dejene, "Characterization of low-temperature-grown ZnO nanoparticles: The effect of temperature on growth," J. Phys. Commun., vol. 6, no. 7, p. 075011, Jul. 2022, doi: 10.1088/2399-6528/ac8049.

[25] D. Mutukwa, R. Taziwa, and L. E. Khotseng, "A Review of the Green Synthesis of ZnO Nanoparticles Utilising Southern African Indigenous Medicinal Plants," Nanomaterials, vol. 12, no. 19, p. 3456, Oct. 2022, doi: 10.3390/nano12193456.

[26] H. Heinz et al., "Nanoparticle decoration with surfactants: Molecular interactions, assembly, and applications," Surf. Sci. Rep., vol. 72, no. 1, pp. 1–58, Feb. 2017, doi: 10.1016/j.surfrep.2017.02.001.

[27] B. Ding et al., "Tuning oxygen vacancy photoluminescence in monoclinic Y_2WO_6 by selectively occupying yttrium sites using lanthanum," Sci. Rep., vol. 5, no. 1, p. 9443, Mar. 2015, doi: 10.1038/srep09443.

[28] C. M. Pelicano, E. Magdaluyo, and A. Ishizumi, "Temperature Dependence of Structural and Optical Properties of ZnO Nanoparticles Formed by Simple Precipitation Method," MATEC Web Conf., vol. 43, p. 02001, 2016, doi: 10.1051/matecconf/20164302001.

[29] A. Jayachandran, A. T. R., and A. S. Nair, "Green synthesis and characterization of zinc oxide nanoparticles using Cayratia pedata leaf extract," Biochem. Biophys. Rep., vol. 26, p. 100995, Jul. 2021, doi: 10.1016/j.bbrep.2021.100995.

[30] S. P. Prakoso and R. Saleh, "Synthesis and Spectroscopic Characterization of Undoped Nanocrystalline ZnO Particles Prepared by Co-Precipitation," Mater. Sci. Appl., vol. 3, no. 8, pp. 530–537, 2012, doi: 10.4236/msa.2012.38075.

[31] G. Baranović and S. Šegota, "Infrared spectroscopy of flavones and flavonols. Reexamination of the hydroxyl and carbonyl vibrations in relation to the interactions of flavonoids with membrane lipids," Spectrochim. Acta A Mol. Biomol. Spectrosc., vol. 192, pp. 473–486, Mar. 2018, doi: 10.1016/j.saa.2017.11.057.

[32] M. Sowmiya, K. Selvam, and M. S. Shivakumar, "Sustainable fabrication of zinc oxide nanoparticles using Secamone emetica leaf extract: Biological and environmental applications," J. Nat. Pestic. Res., vol. 12, p. 100122, Jun. 2025, doi: 10.1016/j.napere.2025.100122.

[33] D. R. Jaishi et al., "Plant-mediated synthesis of zinc oxide (ZnO) nanoparticles using Alnus nepalensis D. Don for biological applications," Heliyon, vol. 10, no. 20, p. e39255, Oct. 2024, doi: 10.1016/j.heliyon.2024.e39255.

[34] L. H. Qian, S. C. Wang, Y. H. Zhao, and K. Lu, "Microstrain effect on thermal properties of nanocrystalline Cu," Acta Mater., vol. 50, no. 13, pp. 3425–3434, Aug. 2002, doi: 10.1016/S1359-6454(02)00155-6.

[35] M. Mahajan et al., "Green synthesis of ZnO nanoparticles using Justicia adhatoda for photocatalytic degradation of malachite green and reduction of 4-nitrophenol," RSC Adv., vol. 15, no. 4, pp. 2958–2980, 2025, doi: 10.1039/D4RA08632E.

[36] M. Abdel-Rahman, H. Ibrahim, M. Y. Mostafa, M. Abdel-Rahman, M. Ebied, and E. A. Badawi, "The characterization of ZnO nanoparticles by applying X-ray diffraction and different methods of peak profile analysis," Physica Scripta, vol. 96, no. 9, p. 095704, 2021.

[37] W. Ahmad and D. Kalra, "Green synthesis, characterization and antimicrobial activities of ZnO nanoparticles using Euphorbia hirta leaf extract," J. King Saud Univ. Sci., vol. 32, no. 4, pp. 2358–2364, 2020.

[38] G. H. Al-Hazmi, M. G. El-Desouky, and A. A. El-Bindary, "Synthesis, characterization and microstructural evaluation of ZnO nanoparticles by Williamson–Hall and size–strain plot methods," Bull. Chem. Soc. Ethiop., vol. 36, no. 4, 2022.

[39] N. S. M. Alnagar, M. Hasanin, W. B. Suleiman, S. A. Zaki, and A. H. Hashem, "Preparation of nanocomposite based on zinc oxide nanoparticles and biopolymers: Characterization, antimicrobial and anticancer activities," Microbial Biosystems, vol. 10, no. 1, pp. 68–81, 2025.

[40] A. M. Awwad, M. W. Amer, N. M. Salem, and A. O. Abdeen, "Green synthesis of zinc oxide nanoparticles (ZnO-NPs) using Ailanthus altissima fruit extracts and antibacterial activity," Chem. Int., vol. 6, no. 3, pp. 151–159, 2020.

[41] E. K. Droepenu, B. S. Wee, S. F. Chin, K. Y. Kok, and M. F. Maligan, "Zinc oxide nanoparticles synthesis methods and its effect on morphology: A review," 2022.

[42] R. R. Gandhi and D. K. Koche, "An insight of zinc oxide nanoparticles (ZnO NPs): Green synthesis, characteristics and agricultural applications," Biosci. Biotechnol. Res. Asia, vol. 21, no. 3, pp. 863–876, 2024.

[43] M. A. L. Grace, K. V. Rao, K. Anuradha, A. J. Jayarani, and A. Rathika, "X-ray analysis and size–strain plot of zinc oxide nanoparticles by Williamson–Hall," Mater. Today Proc., vol. 92, pp. 1334–1339, 2023.

[44] F. Güell et al., "ZnO-based nanomaterials approach for photocatalytic and sensing applications: Recent progress and trends," Mater. Adv., vol. 4, no. 17, pp. 3685–3707, 2023.

[45] H. Hameed et al., "Green synthesis of zinc oxide (ZnO) nanoparticles from green algae and their assessment in various biological applications," Micromachines, vol. 14, no. 5, p. 928, 2023.

[46] N. A. S. M. Idris et al., "Optical and optoelectronic metal oxide-based sensors (optical sensors, principle, computational modeling, and application-based development)," in Metal Oxides for Optoelectronics and Optics-Based Medical Applications, Elsevier, 2022, pp. 151–164.

[47] A. Jayachandran, T. Aswathy, and A. S. Nair, "Green synthesis and characterization of zinc oxide nanoparticles using Cayratia pedata leaf extract," Biochem. Biophys. Rep., vol. 26, p. 100995, 2021.

[48] S. T. Karam and A. F. Abdulrahman, "Green synthesis and characterization of ZnO nanoparticles by using thyme plant leaf extract," Photonics, 2022.

[49] A. U. Khan et al., "Biosynthesis and characterization of zinc oxide nanoparticles (ZnONPs) obtained from the extract of waste strawberry," J. Umm Al-Qura Univ. Appl. Sci., vol. 9, no. 3, pp. 268–275, 2023.

[50] M. Kotresh, M. Patil, and S. R. Inamdar, "Reaction temperature based synthesis of ZnO nanoparticles using co-precipitation method: Detailed structural and optical characterization," Optik, vol. 243, p. 167506, 2021.

[51] A. Kumar, M. Kumar, N. Srivastava, and A. K. Atul, "Nanoscale characterization," in Fundamentals of Low Dimensional Magnets, CRC Press, 2022, pp. 245–268.

[52] K. L. Naidu et al., "Methods for characterization and quantitation of nanomaterials," in Nanomaterials in the Battle Against Pathogens and Disease Vectors, CRC Press, 2022, pp. 83–118.

[53] R. Naik et al., "Characterization of metal oxide nanomaterials," in Advances in Space Radiation Detection: Novel Nanomaterials and Techniques, Springer, 2024, pp. 37–57.

[54] M. U. Rashid et al., "Green synthesis and characterization of zinc oxide nanoparticles using Citrus limetta peels extract and their antibacterial activity against brown and soft rot pathogens and antioxidant potential," Waste Biomass Valorization, vol. 15, no. 6, pp. 3351–3366, 2024.

[55] N. Sedefoglu, "Characterization and photocatalytic activity of ZnO nanoparticles by green synthesis method," Optik, vol. 288, p. 171217, 2023.

[56] Y. Sun, W. Zhang, Q. Li, H. Liu, and X. Wang, "Preparations and applications of zinc oxide based photocatalytic materials," Adv. Sensor Energy Mater., vol. 2, no. 3, p. 100069, 2023.

[57] S. Vyas, "A short review on properties and applications of zinc oxide based thin films and devices: ZnO as a promising material for applications in electronics, optoelectronics, biomedical and sensors," Johnson Matthey Technol. Rev., vol. 64, no. 2, pp. 202–218, 2020.